



City Research Online

City, University of London Institutional Repository

Citation: Cao, X., He, D., Qian, K., Fu, F., Deng, X-F. & Wang, L. (2023). Shear Behavior of Glass FRP Bars-Reinforced Ultra-High Performance Concrete I-Shaped Beams. *Structural Concrete*, 24(1), pp. 1503-1520. doi: 10.1002/suco.202100801

This is the published version of the paper.

This version of the publication may differ from the final published version.

Permanent repository link: <https://openaccess.city.ac.uk/id/eprint/28214/>

Link to published version: <https://doi.org/10.1002/suco.202100801>

Copyright: City Research Online aims to make research outputs of City, University of London available to a wider audience. Copyright and Moral Rights remain with the author(s) and/or copyright holders. URLs from City Research Online may be freely distributed and linked to.

Reuse: Copies of full items can be used for personal research or study, educational, or not-for-profit purposes without prior permission or charge. Provided that the authors, title and full bibliographic details are credited, a hyperlink and/or URL is given for the original metadata page and the content is not changed in any way.

City Research Online:

<http://openaccess.city.ac.uk/>

publications@city.ac.uk

ARTICLE

Shear behavior of glass FRP bars-reinforced ultra-high performance concrete I-shaped beams

Xia Cao^{1,2} | Dabo He^{1,2,3} | Kai Qian¹ | Feng Fu⁴  | Xiao-Fang Deng¹ | Lei Wang¹

¹College of Civil and Architecture Engineering, Guilin University of Technology, Guilin, China

²Guang Xi Key Laboratory of New Energy and Building Energy Saving, Guilin, China

³Nanning College of Technology School of Civil Engineering, Guilin, China

⁴Department of Engineering, School of Science and Technology, City, University of London, London, UK

Correspondence

Feng Fu, Department of Engineering, School of Science and Technology, City, University of London, London, EC1V, 0HB UK.

Email: feng.fu.1@city.ac.uk

Xiao-Fang Deng, College of Civil and Architecture Engineering, Guilin University of Technology, Guilin 541004, China.

Email: dengxiaofang@gult.edu.cn

Funding information

National Natural Science Foundation of China, Grant/Award Number: 52022024; National Natural Science Foundation of Guangxi, Grant/Award Number: 2018GXNSFAA281188; Natural Science Foundation of China, Grant/Award Number: 51968013

Abstract

In this paper, the shear behavior of glass fiber reinforced polymer (GFRP) bars reinforced ultra-high-performance concrete (UHPC) beams was investigated through experimental tests. Eight GFRP bars reinforced UHPC I-beams were tested until shear failure with various stirrup ratio, reinforcement ratio, and shear span to depth ratio. The shear capacity, load–deflection relationship, cracking pattern, and failure mode were investigated in detail. The results show that the shear span to depth ratio has the greatest influence on the shear capacity of the beam among the three parameters, followed by the stirrup ratio and reinforcement ratio. The stirrup configuration can significantly improve the shear capacity and deformation resistance of the beam and can effectively reduce the stress concentration caused by the uneven distribution of steel fibers, which affects the failure mode of the beam. Increasing the stirrup ratio and reinforcement rate can improve the stiffness of the beam after cracking, and the larger the shear span to depth ratio is, the more significant the improvement effect is. Moreover, the stirrup enables the full development of the tensile capacity of GFRP bars. The existing equations of shear strength from five design codes and seven literatures are compared to the experimental results of 54 UHPC beams. It showed that the formula from the codes AFGC-2013 and JSCE-2006 codes is more accurate. The equations by Kwak, Jin, and Thiemicke's provide the best predictions.

KEYWORDS

glass fiber reinforced polymer rebar, shear behavior, shear span to depth ratio, stirrup ratio, ultra-high-performance concrete

Discussion on this paper must be submitted within two months of the print publication. The discussion will then be published in print, along with the authors' closure, if any, approximately nine months after the print publication.

This is an open access article under the terms of the [Creative Commons Attribution-NonCommercial-NoDerivs](https://creativecommons.org/licenses/by-nc-nd/4.0/) License, which permits use and distribution in any medium, provided the original work is properly cited, the use is non-commercial and no modifications or adaptations are made.

© 2022 The Authors. *Structural Concrete* published by John Wiley & Sons Ltd on behalf of International Federation for Structural Concrete.

1 | INTRODUCTION

Fiber reinforced polymer (FRP) has the characteristics of lightweight, high strength, good corrosion resistance, and high tensile strength.^{1,2} It can be used as a substitute for ordinary steel bars in some harsh environments, such as marine structures and chemical storage tank systems. Ultra-high performance concrete (UHPC) is a new type of green and sustainable engineering material with high compactness, durability, and excellent mechanical properties.^{3–5} Structural members using UHPC exhibit better durability, energy dissipation, and fatigue performance compared to conventional concrete members. UHPC with addition of steel fibers has been widely used in certain projects required higher strength,⁶ better seismic performance, and desirable blast resistance.^{7,8} Therefore, it has attracted considerable attention from engineering and academic communities. In addition, Due to its high compressive strength, it is more suitable for prestressed concrete, which can further reduce the weight of the structure components and costs. Thus, UHPC has been widely used in bridge engineering—for example, the 60 m span Sherbrooke Bridge (Quebec, Canada), and 120 m span Senyu Footbridge (Seoul, South Korea).

Since the advent of ultra-high performance concrete in 1990s, in the past decade, extensive studies have been made on the shear capacity of UHPC beams. Wu⁹ and Baby¹⁰ carried out shear capacity tests on I-shaped UHPC beams, and found that the fiber orientation has an important influence on the shear capacity of beams. Moreover, Wu proposed a simplified formulation to predict the first diagonal cracking load and pointed out that the traditional reinforced concrete calculation model is not suitable for ultra-high performance concrete. Chen,¹¹ Xu,¹² and Liang¹³ carried out shear tests on reinforced ultra-high performance concrete beams. The experimental parameters were the volume fraction of steel fiber, shear span to depth ratio, longitudinal reinforcement ratio, and stirrup ratio. The test results indicated that the dosage of steel fiber has the greatest influence on the shear strength of beams and the stirrup ratio has the least influence. However, the stirrup can affect the failure mode of beams. According to the test results and existing UHPC beam shear test data, the shear strength prediction formula based on truss-arch theory is improved. Qi¹⁴ and Xia¹⁵ carried out shear capacity tests on high strength steel (HSS) reinforced ultra-high performance fiber reinforced concrete (UHPRFC) beams. The test results showed that shear span to depth ratio, ratio of the steel fiber, fiber type, concrete strength and stirrup ratio have improved the shear strength and ductility of UHPRFC beams, especially post-cracking shear strength and deformability, of UHPRFC beams. Compared with traditional concrete, the shear failure of HSS-UHPRFC beams

is not brittle, and the stiffness of the UHPRFC beams at ultimate state was about 50% of initial beam stiffness. Voo,^{16,17} Jin et al.,¹⁸ and Zheng¹⁹ tested prestressed RPC I-beams without stirrups. The variables investigated were the type and dosage of fibers, shear span to depth ratio, stirrup ratio, and prestress level. The results show that the steel fiber has bridging effect, and a large number of shear cracks develop in the web before the critical diagonal cracks appear, which improves the shear capacity of the beam, prestressing can effectively improve the cracking load and stiffness of beams. The bond performance of FRP reinforced concrete has been found in^{20,21}

Due to the complexity of shear mechanism of UHPC,²² it is difficult to obtain accepted theoretical calculation formula at present. The French UHPC guideline AFGC-2013,²³ the Japanese UHPC structural design and construction guideline JSCE-2006²⁴ and the Swiss UHPC standard SIA-2016,²⁵ all based on Strut and Tie theory, adopt semi-empirical and semi-theoretical shear strength calculation formulas. Many shear calculation models have been developed by scholars in various countries, including limit equilibrium theory, plasticity theory, Strut and Tie method, pressure field theory and truss-arch theory.²⁶ Kawk,²⁷ Jin Lingzhi,¹⁸ Lim,²⁸ and Thiemicke²⁹ have analyzed and deduced the calculation model of shear strength of UHPC beams without web reinforcement. However, the calculation results of these formulas are different and even contradictory, so the accuracy of the calculation model of shear strength still needs further verification.

At present, scholars from all over the world have mainly studied the shear capacity of UHPC beams without stirrup, while the research on the combination of FRP reinforcement and UHPC is still rare. In view of the high shear capacity of UHPC, there is a tendency to arrange less or even no stirrup in UHPC structural members, however, it may cause brittle shear failure without obvious signs. It is not clear whether the stirrup has great influence on the shear capacity of UHPC beams, especially on the ductility and failure modes of UHPC beams with FRP reinforcement. Based on this, in this paper 8 GFRP bars reinforced UHPC beams without and with stirrup were tested. The shear capacity of UHPC beams is studied with the stirrup ratio, longitudinal reinforcement ratio and shear span to depth ratio as variables.

2 | EXPERIMENTAL METHODS

2.1 | Test specimens

To study the shear capacity of GFRP bars reinforced UHPC beams, eight simply supported I-beams without

and with stirrup were designed and manufactured with the reinforcement ratio ρ_s (1.4%, 2.3%), the stirrup ratio ρ_{sv} (0%, 0.67%) and the shear span to depth ratio $\lambda = a/d$ (1.6, 2.6). The beams without stirrup and those with stirrup were divided into group 1 and group 2. All beams

have the same cross-sectional dimensions. The details of beams of cross-sectional parameters and reinforcement, is shown in Figure 1. The specimens were named follows the rule that $XB-Y-Z$, where X stands for beam length (3700 mm with “S” and 4600 mm with “L”), B stands for

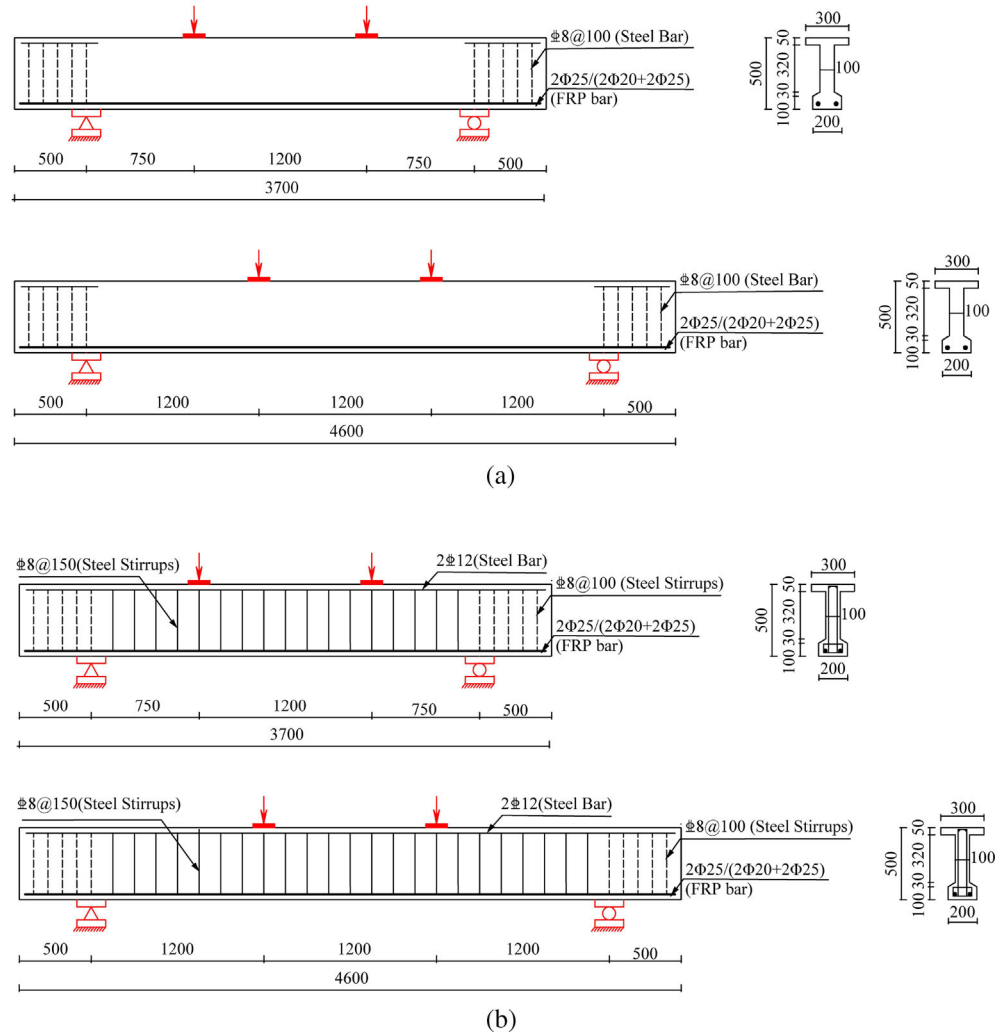


FIGURE 1 Details and reinforcement layout of beams; (a) section size and reinforcement arrangement of beam without stirrup and (b) section size and reinforcement arrangement of beam with stirrup

TABLE 1 Details of GFRP reinforced UHPC beam specimens

Specimen #	Shear span a , mm	Web width b_w , mm	Height h , mm	Tensile reinforcement	Reinforcement ratio, ρ_s %	Stirrup spacing C8 mm	Stirrup ratio ρ_{sv} %	λ
S1-1.4-1.6	750	100	500	2Φ25	1.4	—	—	1.6
S1-2.3-1.6	750	100	500	2Φ20 + 2Φ25	2.3	—	—	1.6
L1-1.4-2.6	1200	100	500	2Φ25	1.4	—	—	2.6
L1-2.3-2.6	1200	100	500	2Φ20 + 2Φ25	2.3	—	—	2.6
S2-1.4-1.6	750	100	500	2Φ25	1.4	150	0.67	1.6
S2-2.3-1.6	750	100	500	2Φ20 + 2Φ25	2.3	150	0.67	1.6
L2-1.4-2.6	1200	100	500	2Φ25	1.4	150	0.67	2.6
L2-2.3-2.6	1200	100	500	2Φ20 + 2Φ25	2.3	150	0.67	2.6

Note: Φ is GFRP reinforcement; C is HRB400 grade steel bar.

TABLE 2 Proportioning of UHPC

Material consumption, kg m ⁻³							
Cement	Quartz sand			Silica fume	Superplasticiser	Steel fiber	Water
	Fine ^a	Medium ^b	Coarse ^c				
1054.6	210.9	843.6	210.9	316.4	21.1	156	242.5

Note: Straight section steel fiber is used, with diameter $D = 0.2$ mm and length $L = 13$ mm.

^aSize 0.16–0.32 mm.

^bSize 0.3–0.6 mm.

^cSize 0.6–1.25 mm.

Test group #	f'_c , MPa	f_c , MPa	f_{cc} , MPa	f_{ts} , MPa	E_c , MPa
1	133.5	114.5	102.2	6.4	45.6
2	136.8	111.9	103.4	6.5	45.3

TABLE 3 Mechanical properties of test specimens

Abbreviations: f'_c , cubic compressive strength; f_c , prism compressive strength; f_{cc} , cylinder compressive strength; f_{ts} , cubic tensile splitting strength; E_c , modulus of elasticity.

presence or absence of web reinforcement (1 means no stirrup, 2 means stirrup), Y stands for longitudinal reinforcement ratio and Z stands for shear span to depth ratio. The specific design parameters of test beam are listed in Table 1.

2.2 | Material properties

2.2.1 | UHPC properties

Test group 1 and 2 beams are casted in the same batch, and the mixture ratio is shown in Table 2. The properties of the test specimen materials are summarized in Table 3. The cubic compressive strength (f'_c) was obtained from 100 mm cubes stressed under load control at a rate of 1.2 MPa/s. The prism compressive strength (f_c) was measured by three (100 × 100 × 300 mm) prisms using a load control method with a rate of 1.2 MPa/s. The cylinder compressive strength (f_{cc}) was obtained from 100 mm cylinders under load control at a rate of 1.2 MPa/s. The cubic tensile splitting strength (f_{ts}) was obtained from tests on three 100 mm cubes at a rate of 0.2 MPa/s. Finally, the modulus (E_c) was also measured, as the stress–strain curve was plotted when the 150 × 150 × 300 mm prisms were tested. All test beams and test blocks shall be cured under the same standard curing conditions, and the test beams and test blocks shall be loaded at the same time.

2.2.2 | GFRP and HRB400 properties

The GFRP bars and HRB400 bars used in the test are produced by Nanjing Feng Hui Composite Material Co., Ltd.

and Jin sheng Steel Co., Ltd., respectively. The details of reinforcing mesh and reinforcing bars are showed in Figure 2. Table 4 shows the mechanical properties of GFRP bars and HRB400 bars measured by standard tensile test.

2.3 | Loading system and measurement scheme

2000 kN hydraulic jack and distribution beam are used to apply symmetrical concentrated load, and JHBU pressure sensor with total range of 1500 kN is used to record the applied load in real time. When the test beam is damaged or the load drops to 80% of the ultimate bearing capacity, the loading process will be stopped. In order to ensure the accuracy of cracking load observed in the early stage of the test and the accuracy of the test curve at the peak load, loading is applied by increment. The loading system is shown in Figure 3, where P_u is the estimated shear strength.

During the test, the following data were collected: (1) Five dial gauges were arranged at the top of the beam at the support, the bottom of the beam at the corresponding loading point and the bottom of the midspan beam to measure the vertical displacement; (2) Four rectangular strain rosette are arranged diagonally from the bearing point at the bottom of the beam to the loading point, five gauges are arranged vertical arrangement of beam midspan, and two gauges are arranged at the top of the beam midspan, so as to measure the concrete strain at the diagonal direction the normal strain and the strain at the top surface; (3) In order to obtain the bending deformation of the beam in the loading process,

FIGURE 2 GFRP reinforcement mesh

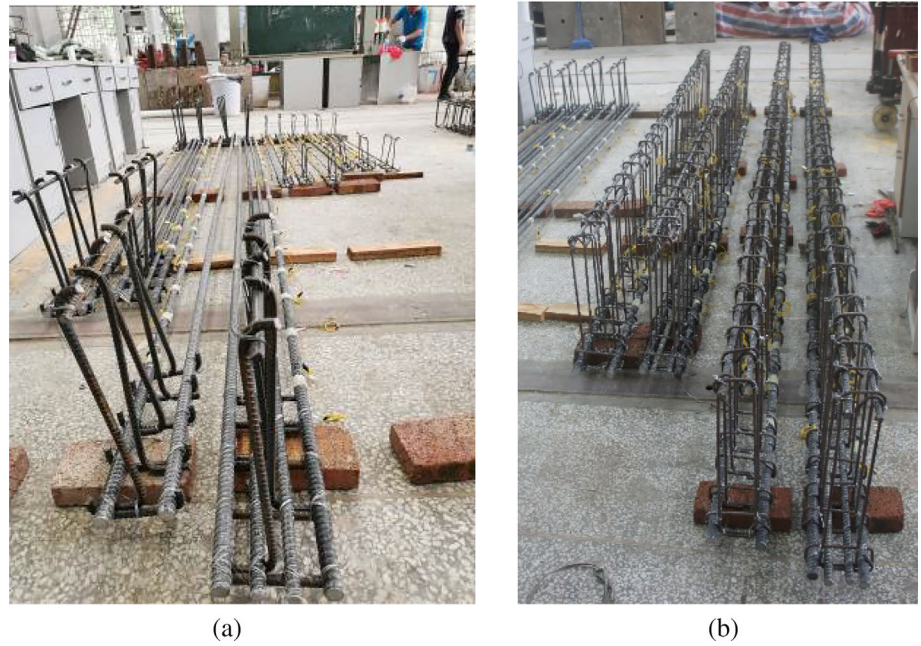
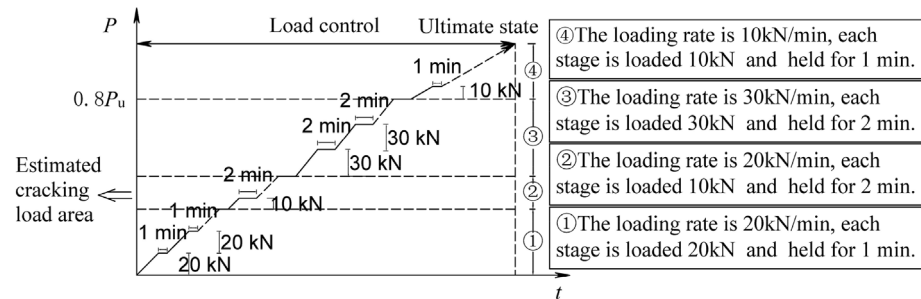


TABLE 4 Mechanical properties of GFRP reinforcement and HRB400 bars

Types	Diameter, mm	Cross sectional area, mm ²	Yield strength, Mpa	Ultimate tensile strength, f_u , Mpa	Elastic modulus, E_f , Gpa	Yield strain, mm/mm	Ultimate strain, mm/mm
GFRP	25	490.9	—	778.4	46.2	—	0.018
GFRP	20	314.1	—	595.3	46.5	—	0.019
HRB400	8	50.3	447.2	648.6	200	0.0022	—

FIGURE 3 Load control



gauges are arranged on the surface of GFRP at the support, the loading point, the midpoint of the shear span and the middle of the span; (4) in the shear span, the gauges are arranged on the surface of stirrup diagonally from the bearing point to the loading point. On the one hand, the contribution of stirrups to the shear resistance of diagonal direction can be examined, on the other hand, more accurate cracking load value can be obtained. (5) The width and cracks patterns on the beam surface under various loads are observed, recorded, and painted. The strain and deflection data of the test beam were collected by the DH3816N static data acquisition system.

The ZBL-F103 crack width observation instrument with a precision of 0.02 mm was used to observe the crack width. The placement of measuring points of LVDT and strain gauges are shown in Figure 4. Similar test setup can be found in³⁰⁻³³

3 | TEST RESULTS AND DISCUSSION

Table 5 provides a summary of the test results. Each characteristic load has considered the deadweight of the test

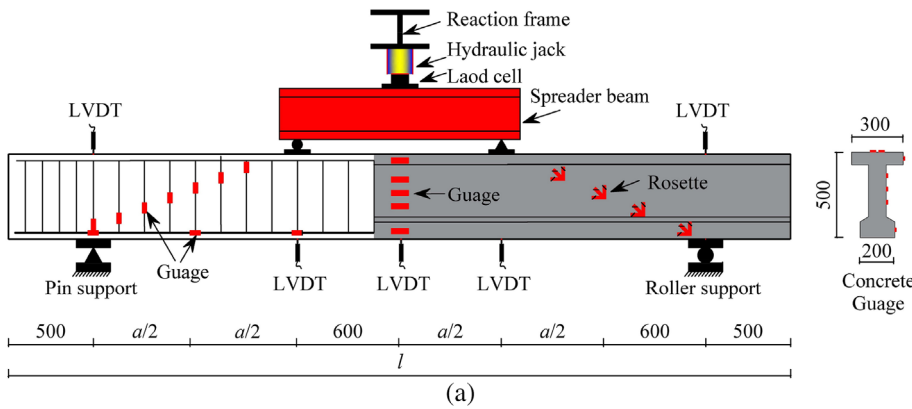


FIGURE 4 Layout of measuring points and test setup; (a) measurement point arrangement and loading device and (b) test setup

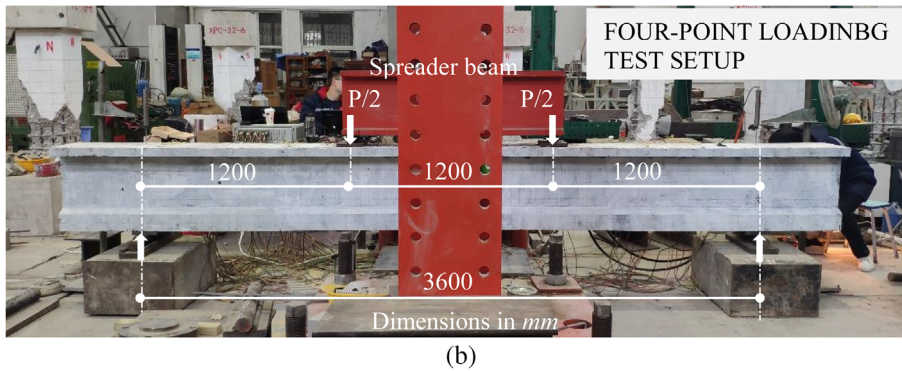


TABLE 5 Test results and failure modes of test beams

Specimen #	$P_{F,cr}$, kN	$P_{D,cr}$, kN	P_u , kN	V_u , kN	Δ_{cr} , mm	Δ_u , mm	Failure mode
S1-2.3-1.6	107.5	380.2	750.2	375.1	12.2	38.05	SCF
L1-1.4-2.6	80.5	226.4	444.2	222.1	18.8	62.4	DTF + STF
L1-2.3-2.6	86.2	305.9	576.1	288.05	22.8	68.1	DTF + STF
S2-1.4-1.6	105.6	345.6	801.4	400.7	12.4	38.5	SCF + SR
S2-2.3-1.6	112.1	401.4	975.2	487.6	12.2	42.6	SCF + SR
L2-1.4-2.6	90.6	275.8	544.3	—	26.7	69.4	RR
L2-2.3-2.6	94.4	311.5	760.4	380.2	20.3	72.4	SCF + SR

Abbreviations: $P_{F,cr}$, flexure cracking load; $P_{D,cr}$, shear cracking load; P_u , peak load; V_u , shear strength ($V_u = P_u/2$); Δ_{cr} , flexure cracking deflection; Δ_u , peak deflection; DTF, diagonal tension failure; RR, reinforcement rupture; SCF, shear compression failure; STF, shear tension failure; SR, stirrup rupture.

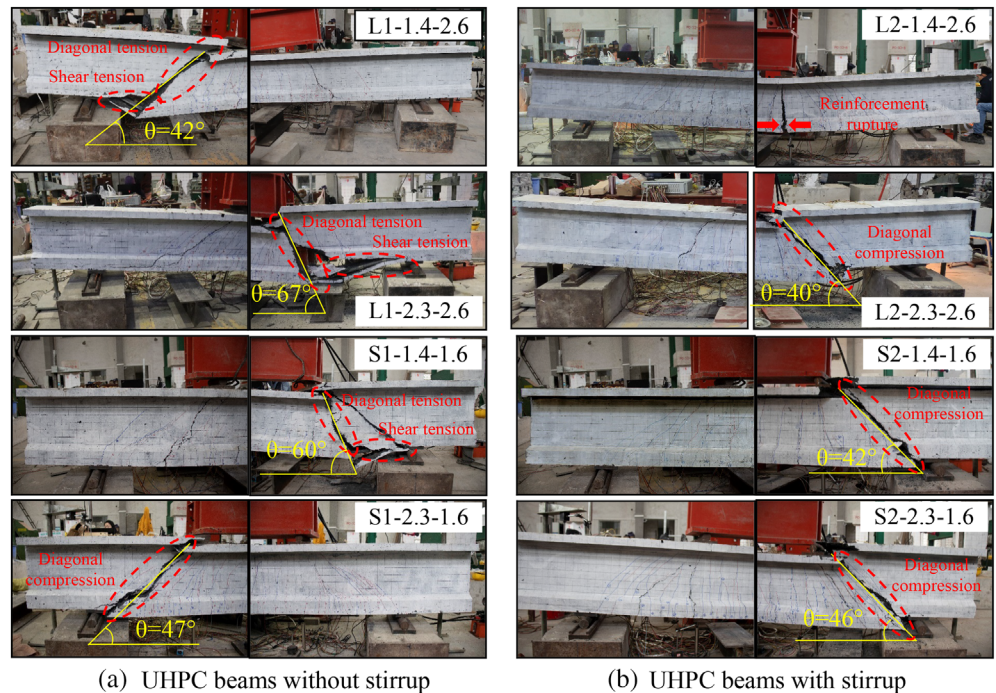
beams. In order to conveniently calculate the influence of diagonal cracks on the shear strength of beams and more accurately compare the cracking performance of beams, the load after the main diagonal cracks is completely formed is defined as the cracking load of shear cracking load. Failure modes are defined based on observing the actual failure of beams.

3.1 | Crack patterns and modes of failure

Figure 5 shows the crack development and failure modes of beams with different longitudinal reinforcement and stirrup ratio. The failure modes of beams are listed in

Table 5. The failure modes of L1-1.4-2.6 and L2-1.4-2.6 beams show that the stirrups prevent the beams from shear failure. This is because the stirrups “bridges” the concrete on both sides of the diagonal crack, effectively preventing the formation of the diagonal crack and limiting its expansion, increasing the dowel action of the GFRP bars and the height of the concrete shear zone, that is, enhancing the shear strength of beams. The development of diagonal cracks is limited by stirrups, while the development of flexural cracks is mainly affected by GFRP bars. Therefore, the arrangement of stirrup improves the shear strength of the beam, which makes its flexural capacity lower than its shear capacity. With the increase of load, the tensile GFRP reinforcement at a

FIGURE 5 Comparison of failure modes of GFRP bars reinforced UHPC beams under different reinforcement ratio and shear span to depth ratio; (a) UHPC beams without stirrup and (b) UHPC beams with stirrup



(a) UHPC beams without stirrup

(b) UHPC beams with stirrup

flexural crack in the pure flexural section of the beam has a strong stress concentration phenomenon compared with other cracks, that is, the tensile deformation of GFRP reinforcement and the width of flexural crack increases rapidly. Finally, the fiber on the surface of GFRP reinforcement is torn, resulting in flexural failure of the beam, such as beam L2-1.4-2.6.

Shear failure were observed for all the UHPC beams except beam L2-1.4-2.6, beams S1-2.3-1.6, S2-1.4-1.6, S2-2.3-1.6, and L2-2.3-2.6 first formed multiple vertical cracks in the pure bending zone and extended to the compression zone as the load increased. Subsequently, many bending-shear type cracks appeared at the bottom of the lower flange in the shear-span zone and a few web-shear type diagonal cracks observed in the middle of the web of beams. Immediately afterwards, a certain web-shear type diagonal crack rapidly extended to the bearing point and loading point, and several parallel diagonal cracks appeared adjacent to it. Finally, after the main diagonal crack is formed, the stirrup is pulled off or the beam is sheared off directly at the main diagonal crack with the sound of the steel fibers being pulled out. Unlike Shear compression failure, diagonal tensile failure in beams (S1-1.4-1.6, L1-1.02-1.6, L1-1.75-1.6) is combined with shear tensile failure. When the lower end of the main diagonal crack develops to the GFRP bar and moves downward under the load, causing the tensile GFRP bar and the diagonal crack to develop horizontally along the skin of the GFRP bar due to bond loss. Resulting in the final failure of the diagonal crack is the main tensile stress-controlled concrete pull-off failure, as

shown in Figure 5. While the diagonal tensile failure is rapid and sudden at the time of failure, without obvious signs of failure.

When shear failure occurs in Figure 5, it is found that after beam is completely broken or the stirrup is pulled off, the UHPC beam is no longer subjected to shear force. The shear force at the main diagonal crack will be resisted entirely by the GFRP bar, which has low modulus of elasticity and poor shear resistance, resulting in the bottom GFRP reinforcement being sheared off instantaneously. Compared with the failure mode of UHPC beams with steel bar under similar conditions, none of the bottom longitudinal bars were sheared off after the shear failure of UHPC beams with steel bar, which was still able to connect the concrete on both sides of the main diagonal crack.³⁴ This indicates that the GFRP bar reinforced UHPC beams are more brittle, less ductile.

It can be observed from Figure 5 that the ranges of the inclination angles of the main diagonal cracks in the test UHPC beams without and with stirrup at the failure are 42° to 67° and 40° to 46° , respectively. The steel fiber distribution has an effect on the shear capacity of the ultra-high performance concrete beams, and the diagonal crack angle depends on the direction of the principal tensile stress, which is influenced by the state of steel fiber distribution. Therefore, the inclination angle of the main diagonal crack in the beams without stirrup is large and random, while the stirrup can weaken the effect of stress concentration generated by the uneven distribution of steel fibers, resulting in a smaller inclination angle of the main diagonal crack in the beams with stirrup and a

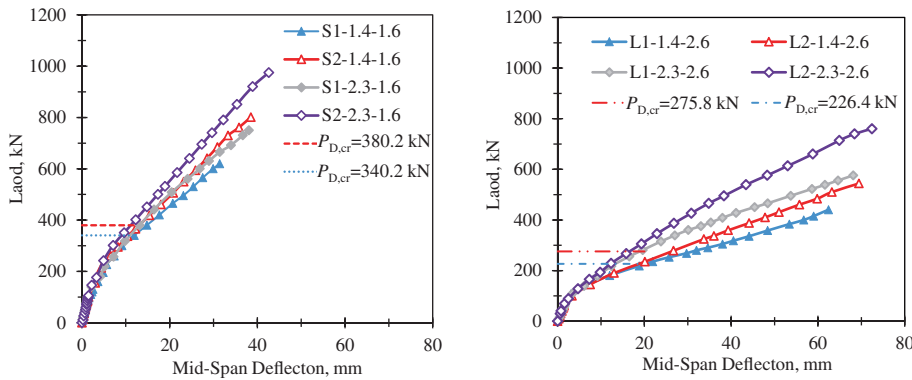


FIGURE 6 Load versus mid-span deflection curve of beam with and without stirrup ($P_{D,cr}$ is the load when the main diagonal crack of the beam without stirrup is fully formed); (a) $L = 3700$ mm and (b) $L = 4600$ mm

tendency to increase with the increase of longitudinal reinforcement ratio.

3.2 | Load–deflection relationship

Figure 6 presents the relationship of mid-span deflection with the applied load for the UHPC beams with and without stirrup. The different longitudinal reinforcement and stirrup ratio are compared in the figure. Generally, the load–deflection curves might be specified into three different stages. The first stage is the pre-cracking stage prior to the occurrence of first flexural crack. In which, the behavior of the curves for the beams with or without stirrup were approximately the same and linear with similar stiffness. The second stage is from the first flexural crack to the full formation of main diagonal cracks. Accompanied by the release of internal energy, the beam stiffness degrades, the slope of the curve decreases significantly, and the stationary point occurs. At this stage, it enters the elastoplastic state, and the deflection curve trend of beams with and without stirrup is still roughly the same. The third stage is the formation of the main diagonal crack until failure occurs, the height of the shear compression zone is basically unchanged, the beam stiffness decays less, and the deflection growth rate remains stable as the load increases. This is consistent with the findings of Yang.³⁵ As can be observed from Figure 6a,b, the slope of the deflection curve decreases for beams without stirrup compared to beams with stirrup, due to the restraint provided by the stirrup for the concrete and longitudinal GFRP bars.

Figure 6a,b shows the decrease of beam mid-span deflection with increasing the longitudinal reinforcement or stirrup ratio for the same load. The slope of the load–deflection curve of the $L = 4600$ mm beam increases more significantly than that of the $L = 3700$ mm beam under the same parameters, which indicates that the stiffness of the $L = 4600$ mm beam is more influenced by the longitudinal reinforcement or stirrup ratio. This is due to

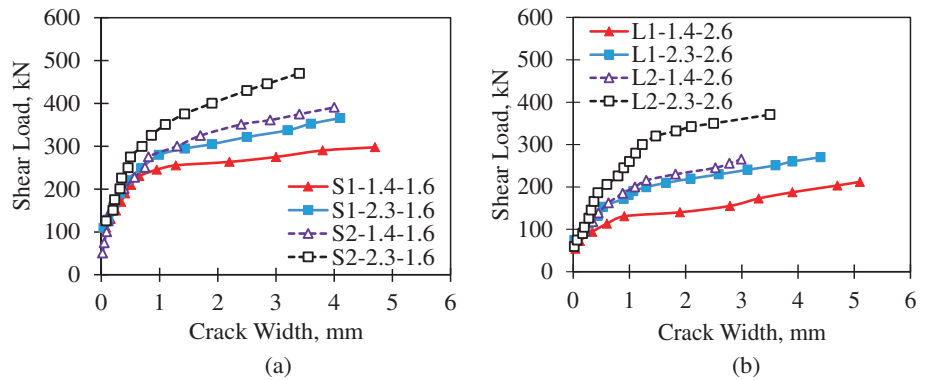
the greater shear span to depth ratio and lower bending line stiffness of the $L = 4600$ mm beam, which results in greater deflection, making the pinning effect of the increased longitudinal reinforcement on the UHPC beam and the restraining effect of the stirrup on the UHPC and GFRP bars more pronounced.

3.3 | Effect of longitudinal reinforcement or stirrup ratio on crack width

Most design codes for steel reinforced concrete structures limit the allowable flexural crack width to protect steel reinforcing bar and stirrup from corrosion and to maintain the durability of the structure. Other reason to control the crack width includes aesthetic and shear effects. The Japan Society of Civil Engineers (JSCE)³⁶ has a maximum allowable crack width limit of 0.5 mm when considering aesthetics only. CAN/CSA S806-12³⁷ allows crack widths of 0.5 mm for exterior exposure and 0.7 mm for interior exposure, while ACI 440-15³⁸ recommends that the CAN/CSA S806-12 limits be used for most cases. However, there is no explicit limit required for the shear diagonal crack width.

The effect of longitudinal reinforcement or stirrup ratio on crack width was considered in this study. Figure 7 shows the relationship between the shear load and the measured main shear diagonal crack width. From Figure 7a, it can be seen that the shear diagonal crack width of $L = 3700$ mm beam decreases with increasing longitudinal reinforcement or stirrup ratio at the same load, and the effect of stirrup ratio is more obvious. This is because the HRB400 stirrup restricts the development of microcracks inside the concrete, thus limiting the crack width on the surface of the beam. From Figure 7b, it is found that the crack development pattern of $L = 4600$ mm beam and the effect of longitudinal reinforcement or stirrup ratio on shear diagonal crack are basically the same as those of $L = 3700$ mm beam,

FIGURE 7 Load versus crack width curve of beam shear crack; (a) beam of $L = 3700$ mm and (b) beam of $L = 4600$ mm



but the slope of shear load-shear diagonal crack width curve of $L = 4600$ mm beam is smaller as well as the maximum crack width is larger after the diagonal crack is fully formed, that is, the stiffness loss and deformation of $L = 4600$ mm beam are larger.

The shear diagonal crack widths measured at 90% of the ultimate load for S1-1.4-1.6, S1-2.3-1.6, S2-1.4-1.6, S2-2.3-1.6, L1-1.4-2.6, L1-2.3-2.6, L2-1.4-2.6 and L2-2.3-2.6 are 3.8, 3.2, 2.9, 2.5, 4.7, 3.9, 2.45 and 2.1 mm. In addition, the decreases in the width of the main shear diagonal crack with increasing longitudinal reinforcement ratio were 15.8% and 13.8% for the beams without and with stirrup at $L = 3700$ mm, respectively, while the decreases were 17.0% and 14.3% for the beams without and with stirrup at $L = 4600$ mm, respectively. The decreases in the width of the main shear crack with increasing reinforcement ratio for the beams with low and high reinforcement ratio at $L = 3700$ mm. The main shear diagonal crack width of beams with low reinforcement ratio and high reinforcement ratio of $L = 3700$ mm decreases by 23.7% and 21.9% respectively with the increase of stirrup ratio, while that of beams with low reinforcement ratio and high reinforcement ratio of $L = 4600$ mm decreases by 47.9% and 46.2% respectively, which shows that the diagonal crack width of beams with low reinforcement ratio is more affected by stirrup ratio and the restraining effect of stirrup on diagonal crack is more obvious.

3.4 | Reinforcement and concrete strain

Figure 8 shows the relationship between load and GFRP reinforcement mid-span strain and concrete strain at the top of the span for GFRP reinforced UHPC beams without and with stirrup. Generally, the load-strain curves of GFRP bars and concrete for GFRP reinforced UHPC beams with and without stirrup follow the same trend in their load-span deflection curve. Before cracking, the load-strain curves are approximately linear, while the

beam stiffness suddenly decreases after concrete cracking. The slope of the corresponding load-strain curves suddenly decreases and the curves show a turning point. It is clearly seen from Figure 8a,b that the concrete and GFRP reinforcement strains of the configured stirrup and the corresponding no stirrup beams follow the same development trend, while the concrete and GFRP reinforcement strains decrease with increasing reinforcement ratio under the same load. This is because the height of the concrete shear compression zone increases significantly with the increase of the longitudinal reinforcement ratio after beam cracking, resulting in a higher stiffness of the high reinforcement beam than the low reinforcement beam.

In addition, the tensile strains of GFRP bars in the range of 9246.2–12,965.4 $\mu\epsilon$ and 13,959.0–16,014.1 $\mu\epsilon$ for the beams with $L = 3700$ mm and 4600 mm under shear damage, respectively. This indicates that the tensile strains of GFRP bars in shear damage do not reach the ultimate tensile strains and are 51.37%–72.03% of the ultimate strains and 77.55%–88.97%. This is due to the fact that the beam is designed for shear damage before bending damage. In contrast, the L2-1.4-2.6 beam suffered bending damage due to insufficient reinforcement ratio, and the maximum strain of GFRP bars was 17065.5 $\mu\epsilon$, which had reached the ultimate tensile strain. It is noteworthy that the strain of GFRP tendons changes greatly when the shear damage occurs in the beam configured with stirrup, and the tensile properties are fully utilized. However, after the damage, the GFRP tendons fracture directly, and the beam has no excess bending deformation performance and excessive brittleness.

3.5 | Load-strain of stirrup

Figure 9 shows the shear load-stirrup strain relationship for the GFRP reinforced UHPC with stirrup strain beam. As shown in the figure, the curve can be divided into three stages, the stirrup strain grows linearly and not

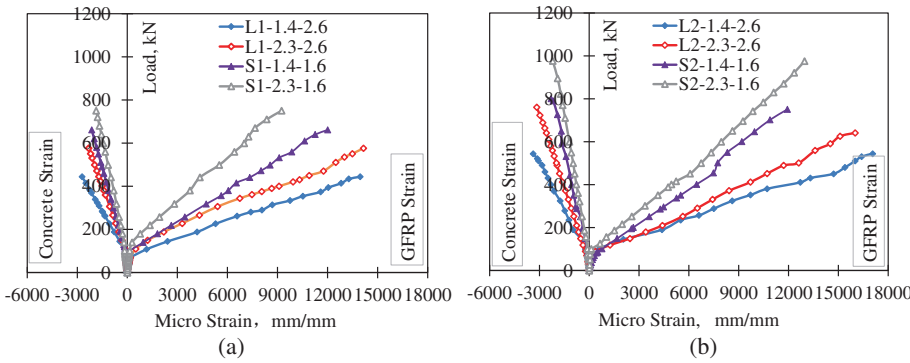


FIGURE 8 Load versus mid-span concrete and GFRP strains for beams with and without stirrup; (a) beams without stirrup and (b) beams with stirrup

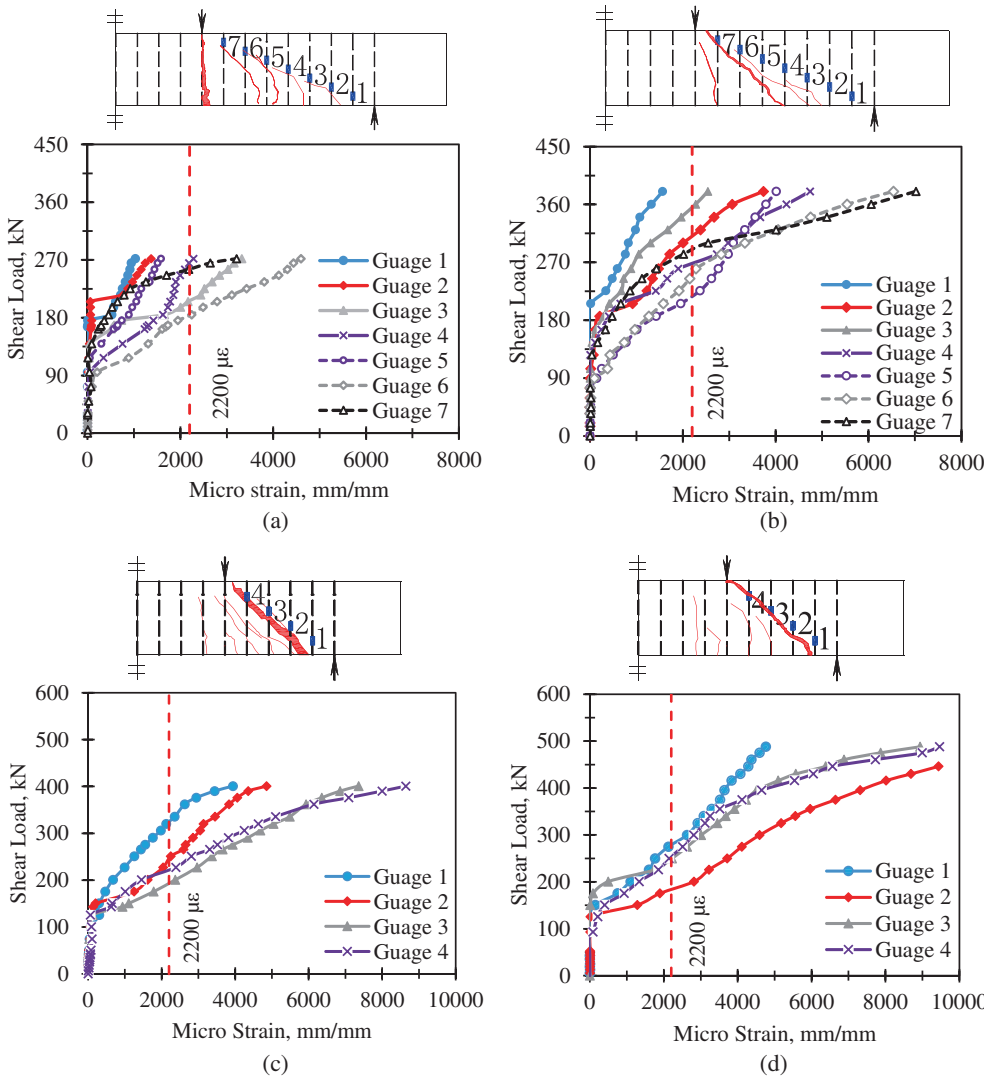


FIGURE 9 Shear load–stirrup strain curves for GFRP reinforced UHPC beams with stirrup; (a) L2-1.4-2.6; (b) L2-2.3-2.6; (c) S2-1.4-1.6; and (d) S2-2.3-1.6

more than $100\mu\epsilon$ from the early stage of loading to the appearance of the shear diagonal crack. After the appearance of the shear diagonal crack, the stirrup strain increases suddenly, but because of the bridging effect of the steel fibers in the UHPC at this time, the crack width is small, that is, the UHPC can still withstand a certain tensile stress after cracking, and the stirrup strain grows slowly. When the critical shear diagonal crack is formed,

with the increase of the crack width, the steel fibers are continuously pulled out, the shear force on the stirrup is gradually increased, and the stirrup strain increases sharply. When the ultimate load is approached, the stirrup strain increases to $7000\text{--}9000\mu\epsilon$, then gradually increases until the stirrup is pulled out and the beam is Shear compression failure. Moreover, combined with the damage modal diagram, it can be observed that the main

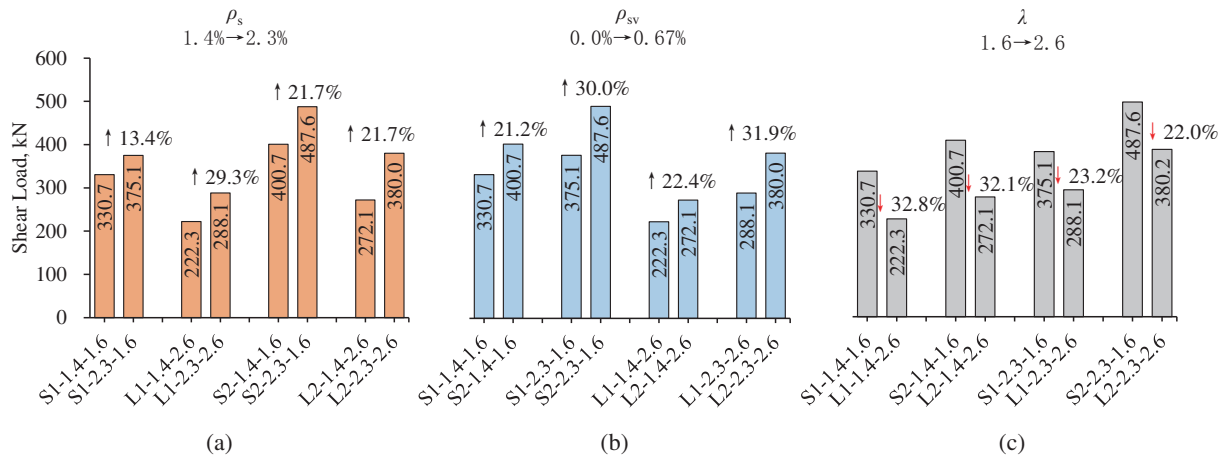


FIGURE 10 Impact of different longitudinal reinforcement ratio, stirrup ratio and shear span to depth ratio on shear behavior of GFRP reinforced UHPC beams; (a) longitudinal reinforcement ratio; (b) stirrup ratio; and (c) shear span to depth ratio

deformation of the stirrup is at the shear diagonal crack, and the closer the stirrup strain gauges are to the main diagonal crack, the higher the strain value is, and the sudden increase of strain only occurs at the stirrup intersecting with the shear diagonal crack. The strains in the stirrups of the $L = 4600$ mm beams are smaller compared to those of the $L = 3700$ mm beam. This is because the Shear-to-span ratio of the $L = 4600$ mm beam is relatively large, the shear span section is longer, and the inclination angle of the main diagonal crack at the time of beam failure is around 40° , and there are more stirrups reinforcement intersecting the diagonal crack. According to Figure 9b, we can see that stirrup gauges 1–4 are not at the main diagonal crack, so the strain of stirrup gauges 1–4 is smaller.

3.6 | Effect of different parameters on shear strength of UHPC beams

Figure 10 shows the effect of different longitudinal reinforcement ratio, stirrup ratio and shear-to-span ratio on the shear strength of GFRP-reinforced UHPC beams. According to Figure 10a, it can be seen that for beams with shear-to-span ratio of $\lambda = 1.6$ ($\lambda = 2.6$), the shear strength of beams without and with stirrup at high reinforcement ratio increased by 13.4% and 21.7% (29.6% and 39.7%), respectively, compared to beams with low reinforcement ratio. This indicates that the pinning action of the longitudinal reinforcement has an effect on the shear strength of the UHPC beam and the contribution of the longitudinal reinforcement should be properly considered in the calculation model. In Figure 10b, it is shown that the configuration of stirrup increases the shear strength of beam with longitudinal reinforcement ratio of

$\rho_s = 1.4\%$ and $\rho_s = 2.3\%$ by 21.2% and 30.0% (22.4% and 31.9%) for a shear-to-span ratio of $\lambda = 1.6$ ($\lambda = 2.6$), respectively. This is due to the fact that stirrup is one of the main factors affecting beam shear strength, and the ability to limit cracks by stirrup, the beam shear strength with stirrup is greatly improved. The data in Figure 10c show that the shear strength of beams without stirrup (with stirrup) with reinforcement ratio of $\rho_s = 1.4\%$ and $\rho_s = 2.3\%$ is reduced by 32.8% and 23.2% (32.1% and 22.0%), respectively, when the shear-to-span ratio is increased from 1.6 to 2.6. The analysis shows that what is really related to shear failure is the diagonal tensile stress generated by the combination of shear stress and longitudinal bending positive stress. Increasing the reinforcement rate can effectively reduce the longitudinal bending stress, so increasing the reinforcement rate can weaken the effect of shear-to-span ratio.

4 | COMPARISONS OF EXISTING EQUATIONS FROM THE CODES AND AVAILABLE LITERATURE

As the shear damage mechanism of reinforced concrete beams is very complex. There are many factors affecting the shear strength, and these factors are also correlated to each other, and some factors cannot be derived from the exact quantitative relationship. Therefore, it is very difficult to accurately predict the shear strength of the beams. The shear strength of UHPC beams has further complication, due to the need to include the contribution of the “bridging” effect of the steel fibers to the shear strength of the beams, which further increases the complexity of the calculation model from the mechanical theory. Therefore, based on the experimental data in this paper

TABLE 6 Shear strength models of UHPC beams for different codes and proposed equations

Source	Shear strength models	Parameters
ACI318M-14 ⁴⁰	$V_u = \left[\sqrt{f'_c} + 120\rho_s \left(\frac{d}{a} \right) \right] \frac{b_w d}{7} + \frac{A_{sv} f_{yv} d}{s}$	f'_c is the cubic compressive strength; ρ_s is the longitudinal reinforcement ratio; a , b_w and d are the length of the shear span, effective width and effective depth of beam, respectively; A_{sv} is cross sectional area of stirrup; f_{yv} is the yield strength of stirrup; s is stirrup spacing.
AFGC-2013 ²³	$V_{Rd} = \frac{0.21}{\gamma_{cf} \gamma_E} \sqrt{f_{cc}} b_w d + \frac{b_w z \sigma_{Rd,f}}{\tan \theta} + \frac{A_{sv} f_{yv} z}{s}$ $\sigma_{Rd,f} = \frac{1}{K} \frac{1}{\omega_{lim}} \int_0^{\omega_{lim}} \sigma(\omega) d\omega$	$\gamma_{cf} \gamma_E$ is the structural safety factor, generally taken as 1.5; f_{cc} is cylinder compressive strength; z is the length of the internal force arm, taken as $z = 0.9d$; $\sigma_{Rd,f}$ is the residual tensile strength of UHPC fiber; K is the influence factor considering the direction of steel fiber, generally taken as 1.0; ω_{lim} denotes the limit value of crack width; $\sigma(\omega)$ denotes the relationship between UHPC crack width and tensile stress; θ is the angle between the principal compressive stress and the beam axis.
Eurocode 2 ⁴¹	$V_{Rd} = \left[0.18k(100\rho_s f'_c)^{1/3} \right] b_w d + \frac{A_{sv} f_{yv} z}{s} \cot \theta$	$k = 1 + \sqrt{200/d}$, other parameters are the same as the above specifications.
JSCE-2006 ³⁶	$V_u = \frac{0.18}{\gamma_b} \sqrt{f_{cc}} b_w d + \frac{f_{vd} b_w z}{\gamma_b \tan \theta} + \frac{A_{sv} f_{yv} z}{s}$	f_{vd} is the design ensile strength of UHPC at shear diagonal cracks, other parameters with the above specifications.
SIA-2016 ²⁵	$V_{Rd} = V_{Rd,U} + V_{Rd,S}$ $V_{Rd,U} = \frac{0.5 b_w z (f_{Uted} + f_{Utud})}{\tan \theta}$ $V_{Rd,S} = \frac{A_{sv}}{s} \cdot z \cdot f_{yv} \cdot (\cot \theta + \cot \beta) \cdot \sin \beta$ $f_{Uted} = \frac{\eta_t \cdot \eta_{hU} \cdot \eta_k \cdot f_{Utek}}{\gamma_U}, f_{Utud} = \frac{\eta_t \cdot \eta_{hU} \cdot \eta_k \cdot f_{Utuk}}{\gamma_U}$	β is the angle between stirrup and beam axis; f_{Uted} and f_{Utud} are tensile elastic ultimate strength and tensile strength of UHPC, respectively; where η_t is a reduction factor (generally 1.0) considering the length of load action, η_{hU} and η_k are a fiber distribution coefficient considering the thickness of test specimen and casting process, respectively; γ_U is a partial coefficient of structural safety; f_{Utek} and f_{Utuk} are the tested standard values of tensile elastic ultimate strength and tensile strength of UHPC. Other parameters are the same as above.
Kwak et al. ²⁷	$v_u = \left[2.1 \cdot e \cdot f_{spfc}^{0.7} \left(\rho_s \frac{d}{a} \right)^{0.22} + 0.8 v_b^{0.97} \right] b_w d + \frac{A_{sv} f_{yv} z}{s}$	e is arch action factor (1 for $a/d > 3.5$ and $3.5d/a$ for $a/d > 3.5$); f_{spfc} is computed value of split tensile strength of concrete ($f_{spfc} = f'_c / (20 - \sqrt{F}) + 0.7 + \sqrt{F}$, $v_b = 0.41 \cdot \tau \cdot F$); τ represents the average bond stress between straight steel fiber and matrix; referring to the research results of Ali et al. ⁴² ($\tau = 0.6 \sqrt{f_{cc}}$); F is the fiber factor ($F = (L/D) \cdot \rho_f \cdot d_f$); L and D are the length and diameter of steel fiber respectively, d_f is bond factor of steel fiber (0.5 for straight, 0.75 for crimped, 1.0 for hooked).
Ashour ³⁹	$v_u = (2.11 \cdot \sqrt[3]{f_{cc}} + 7F) \left[\rho_s (d/a)^{1/3} \right] b_w d + \frac{A_{sv} f_{yv} z}{s}$	Same parameters as above.
Thiemicke ²⁹	$V_u = V_c + V_s + V_f$ $V_c = \left[\frac{0.15}{\gamma_1} k_1 (100\rho_s f'_c)^{1/3} \right] b_w d$ $V_s = k_2 f_y z \cot(\theta)$ $V_f = f_t b z \cot(\theta)$	γ_1 design safety factor contributing to UHPC shear strength; k_1 is prestress enhancement coefficient, and reinforced concrete is taken as 1.0; k_2 is the calculation coefficient of stirrup's contribution to shear strength; Other parameters are the same as above.
Jin ¹⁸	$V_u = \left(\frac{0.07}{\lambda - 0.852} + \frac{49.086\rho_s}{f_{cc}} \right) f_{cc} b_w d (1 + \beta_f \rho_f)$ $\left(0.755 + 0.054A_d \right) + \frac{A_{sv} f_{yv} z}{s}$	λ is the shear span to depth ratio; β_f is the influence coefficient of steel fiber on shear strength; ρ_f is the volume ratio of steel fiber; A_d is the shape adjustment factor ($A_d = \lambda$ for $1.0 < \lambda < 2.5$, $A_d = 2.5$ for $\lambda \geq 2.5$), refer to Rebeiz. ⁴³

TABLE 7 Characteristics of beams used for comparison of design methods

Reference	No.	f'_c , MPa	f_{cc} , MPa	b_w , mm	d , mm	λ	ρ_s , %	θ	A_{sv} , mm ²	s , mm	f_{yv} , MPa	ρ_f , %	V_{exp}
This study	1	133.5	102.2	100	465	1.60	1.4	60°	—	—	—	2	330.7
	2	133.5	102.2	100	465	1.60	2.3	60°	—	—	—	2	375.0
	3	133.5	102.2	100	465	1.60	1.4	50°	—	—	—	2	222.3
	4	133.5	102.2	100	465	1.60	2.3	67°	—	—	—	2	288.1
	5	136.8	103.4	100	465	1.60	1.4	50°	100.5	150	447	2	400.5
	6	136.8	103.4	100	465	1.60	2.3	45°	100.5	150	447	2	487.6
	7	136.8	103.4	100	465	1.60	2.3	40°	100.5	150	447	2	380.2
Altug Yavas ³⁴	8	121	96.8	50	225	3.10	0.8	35°	—	—	—	0	22.9
	9	121	96.8	50	225	3.10	1.2	38°	—	—	—	0	21.6
	10	121	96.8	50	225	3.10	1.7	40°	—	—	—	0	25.3
	11	121	96.8	50	225	3.10	2.2	45°	—	—	—	0	33.4
Zagon ⁴⁴	12	137.6	110.1	60	380	2.50	3.16	32°	—	—	—	1	121.0
	13	137.6	110.1	60	380	2.50	3.16	35°	—	—	—	1	160.0
	14	137.6	110.1	60	380	2.50	3.16	45°	—	—	—	1	70.0
	15	137.6	110.1	60	380	2.50	3.16	38°	—	—	—	1	129.0
	16	137.6	110.1	60	380	2.50	3.16	47°	—	—	—	1	119.0
	17	137.6	110.1	60	380	2.50	3.16	45°	—	—	—	1	189.0
	18	137.6	110.1	60	380	2.50	3.16	45°	—	—	—	1	80.0
	19	137.6	110.1	60	380	2.50	3.16	40°	—	—	—	1	154.0
Tamas meszoly ⁴⁵	20	185.2	166.7	60	310	3.2	5.1	33°	157.1	125	594	2	540.0
	21	184.2	165.8	60	310	3.2	5.1	35°	157.1	125	594	2	578.0
	22	154.3	138.9	60	310	3.5	5.1	31°	157.1	125	594	0	337.0
	23	172.9	155.6	60	310	3.5	5.1	32°	157.1	125	594	0	369.0
	24	169.7	152.7	60	310	3.5	5.1	33°	157.1	200	594	2	443.0
	25	162.8	146.5	60	310	3.5	5.1	29°	157.1	200	594	2	516.0
	26	169.8	152.8	60	310	3.5	5.1	33°	157.1	200	594	1	445.0
	27	168.2	151.4	60	310	3.5	5.1	30°	157.1	200	594	0	300.0
	28	170.4	153.4	60	310	3.5	5.1	30°	157.1	300	594	2	446.0
	29	165.6	149.0	60	310	3.5	5.1	31°	157.1	300	594	1	398.0
	30	174.9	157.4	60	310	3.5	5.1	30°	157.1	300	594	0	253.0
	31	160.8	144.7	60	310	3.5	5.1	23°	—	—	—	0	82.0
	32	169.6	152.6	60	310	3.5	5.1	30°	—	—	—	0	63.0
	33	166.6	149.9	60	310	3.5	5.1	33°	—	—	—	0	51.0
Jin ¹⁸	34	133.1	106.5	70	350	2.0	2.9	35°	—	—	—	0.75	224.1
Xu ¹²	35	141	126.9	120	320	1.73	6	47°	157.1	500	572	4.5	706
	36	122	109.8	120	320	2.08	6	45°	157.1	300	572	4.5	431
	37	122	109.8	120	320	2.08	6	40°	157.1	200	572	4.5	511
Chen ¹¹	38	108.2	97.38	150	275	1.2	5.23	40°	56.5	200	465.7	0	445
	39	118	106.2	150	275	1.2	5.23	33°	56.5	200	465.7	1	645
	40	132.3	119.07	150	275	1.2	5.23	37°	56.5	200	465.7	2	720
	41	164.8	148.32	150	275	1.2	5.23	31°	56.5	200	465.7	3	845
	42	118	106.2	150	275	1.2	5.23	41°	56.5	200	465.7	1	580

(Continues)

TABLE 7 (Continued)

Reference	No.	f'_c , MPa	f_{cc} , MPa	b_w , mm	d , mm	λ	ρ_{ss} , %	θ	A_{sv} , mm ²	s , mm	f_{yv} , MPa	ρ_f , %	V_{exp}
Yang ³⁵	43	118	106.2	150	275	1.2	5.23	38°	56.5	100	465.7	1	
	44	118	106.2	150	275	1.2	5.23	35°	56.5	150	465.7	1	655
	45	118	106.2	150	275	1.2	5.23	38°	56.5	200	465.7	1	560
	46	118	106.2	150	275	1.2	5.23	42°	56.5	200	465.7	1	490
	47	118	106.2	150	275	1.4	5.23	33°	56.5	200	465.7	1	525
	48	118	106.2	150	275	1.6	5.23	45°	56.5	200	465.7	1	475
	49	174.5	157.05	50	640	2.5	1.17	30°	—	—	—	1	488
	50	188.2	169.38	50	640	2.5	1.17	30°	—	—	—	1.5	527
	51	185.5	166.95	50	640	2.5	1.17	46°	—	—	—	2	712
	52	168.9	152.01	50	640	3.4	1.17	55°	—	—	—	1	279
	53	193	173.7	50	640	3.4	1.17	30°	—	—	—	1.5	404
	54	188.5	169.65	50	640	3.4	1.17	44°	—	—	—	2	437

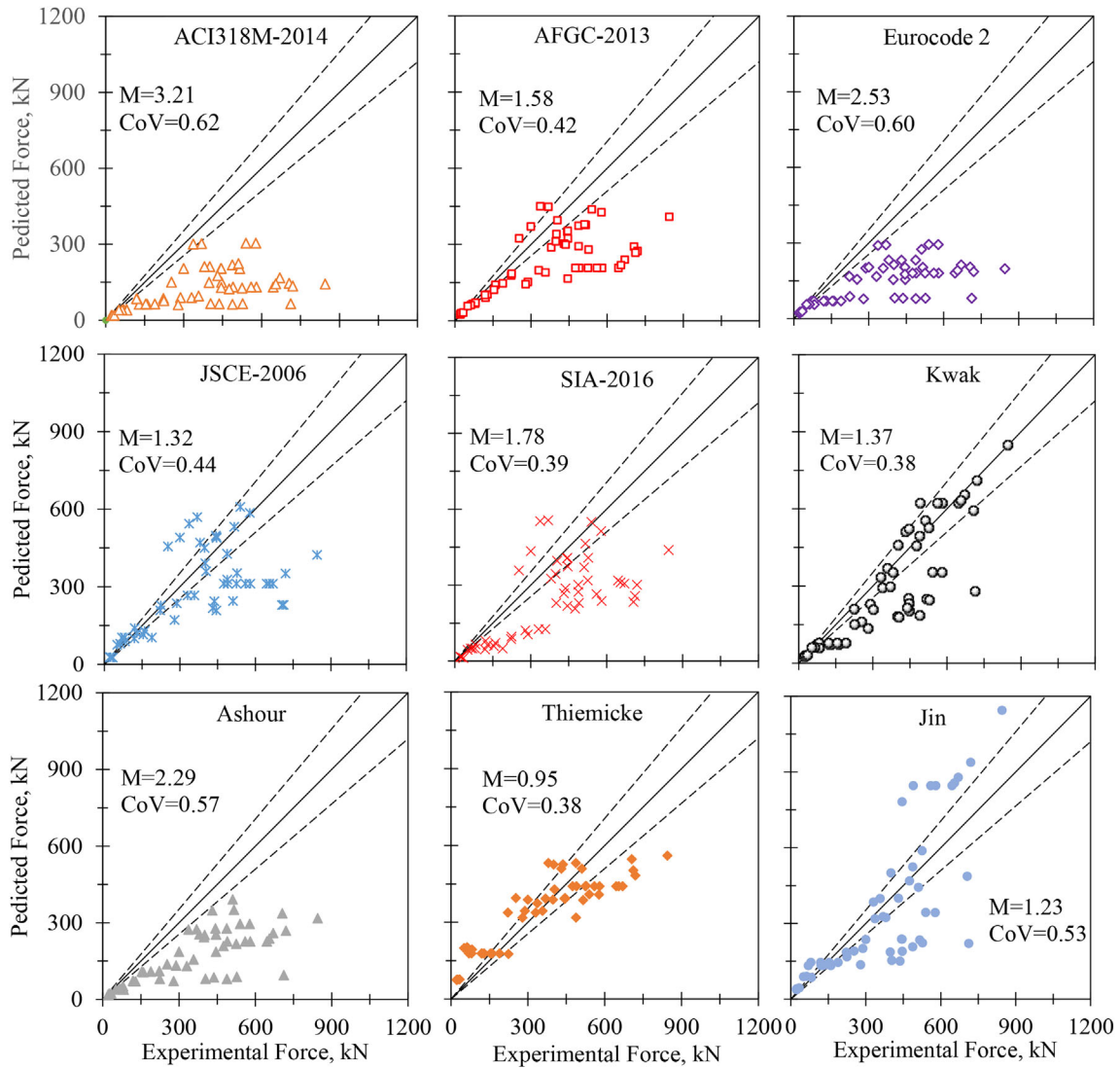


FIGURE 11 Correlations of V_{exp} and V_{cal}

TABLE 8 Analysis of influencing factors of the design methods

Design methods	Mean	COV	Influencing factors			
			UHPC matrix	Steel fiber	Longitudinal bar	Size effect
ACI318-14	3.21	0.62	√	×	√	×
AFGC-2013	1.58	0.42	√	√	×	×
Eurocode 2	2.53	0.6	√	×	√	√
JSCE-2006	1.32	0.44	√	√	×	×
SIA-2016	1.78	0.39	√	√	×	×
Kawk	1.37	0.38	√	√	√	×
Ashour	2.29	0.57	√	√	√	×
Thiemicke	0.95	0.38	√	√	√	√
JIN	1.23	0.53	√	√	√	×

and the experimental data of other scholars, the formulas of UHPC from codes of many countries and many scholars' are compared and analyzed.

Table 6 gives the formula of shear strength of UHPC beams for different codes and available literature. For the no stirrup beams, the calculation formula mainly considered the “bridging” effect of UHPC and steel fibers. For the contribution of stirrup, the calculation formula is basically the same, that is, therefore, on the basis of the shear strength calculation model for beams without stirrup by Kwak,²⁴ Ashour,³⁴ and Jin,¹⁵ the shear strength calculation model for beams with stirrup can be obtained by adding the web calculation formula. Except for ACI318M-14³⁵ and Eurocode 2,³⁶ all the calculated models consider the contribution of steel fiber “bridging” to the shear strength of beams, and the results of Altug Yavas³⁴ and Yang et al.³⁵ showed that the shear strength of beams can be increased by 120%–200% for dosage of steel fibers from 0% to 2.0%, so the steel fibers are not negligible in the shear resistance of beams.

The test results of 7 beams from this study and 47 beams from the literature of 7 different scholars were used to validate the calculated models of ACI318M-14, AFGC-2013, Eurocode 2, JSCE-2006, Swiss SIA-2016, Kwak, Ashour, Thiemicke, and Jin. Table 7 lists the parameters and shear strength of 54 ultra-high performance concrete beams with long straight steel fiber and in the range of 0% to 2% admixture for all beams. Figure 11 shows the correlation between the calculated and tested values of shear strength for 54 beams with different codes and proposed equations. The calculated values do not take into account the safety factor in order to better reflect the accuracy of the code calculation formula. The diagonal solid line in the figure indicates the line with zero tolerance (i.e., $V_{cal} = V_{exp}$) and the diagonal dashed line indicates the line with 15% tolerance

($V_{cal} = 0.85V_{exp}$, $V_{cal} = 1.15V_{exp}$). The correlation between the predicted and experimental values of each computational model can be clearly seen in Figure 11.

The influencing factors of design methods are summarized in Table 8. The reasons for the large variability of the calculation results of design methods are derived through analysis and comparison. The main statistical parameters are mean and coefficient of variation (COV), the former is an indication of accuracy but cannot be relied upon to measure the accuracy as it is varied based on safety margins of the design equations, while the latter is a measure of precision.

1. The mean value of V_{exp}/V_{cal} of ACI318M-14 and Eurocode 2 are 3.21 and 2.53 respectively, and the COV are 0.62 and 0.60 respectively. ACI318M-14 and Eurocode 2 codes are applicable to ordinary concrete below C80, but the strength of concrete in this test is much greater than C80. The difference between ordinary concrete matrix and UHPC matrix is large, these design equations does not consider the bridging effect of steel fiber, and the calculation results are too conservative and the dispersion is the largest, which is not suitable to be applied to the prediction of shear strength of UHPC beam.
2. The mean value of V_{exp}/V_{cal} of Ashour's equation is 2.29 and the COV is 0.57. This theoretical formula is based on the derivation of high-strength fiber concrete, which underestimates the shear contribution of UHPC and needs further study.
3. The mean value of V_{exp}/V_{cal} of AFGC-2013 and SIA-2016 are closer to 1 than those of ACI318M-14, Eurocode 2 and Ashour, with mean values of 1.58 and 1.78, respectively, and COV of 0.42 and 0.39, respectively, which are more conservative predictions. These design equations consider the contribution of UHPC

matrix and steel fiber to the shear strength, but do not consider the influence of longitudinal reinforcement. This study shows that the longitudinal reinforcement has a greater influence on the shear strength of UHPC beams.

4. The mean value of V_{exp}/V_{cal} of JSCE-2006 code is 1.32, and the COV is 0.44. This theoretical formula is optimized based on the shear strength of AFGC-2002 specification, considering the bridging effect of UHPC matrix and steel fiber on the shear contribution. The prediction result of JSCE-2006 is in good agreement with the test value, and the dispersion is relatively good.
5. The mean value of V_{exp}/V_{cal} of Jin's equation is 1.23 and the COV is 0.53. This theoretical formula is obtained by using a semi-empirical and semi-theoretical method, taking into account the factors such as UHPC matrix, steel fibers and longitudinal reinforcement, etc., and the mixture ratio of test specimens in Jin's paper is the same as that in this paper. Therefore, the predicted values of this calculation model match with the test values, but some of the data dispersion is large.
6. The mean value of V_{exp}/V_{cal} of Kwak and Thiemicke's equations are 1.37 and 0.95 respectively, and COV are 0.38 and 0.38 respectively. These theoretical formulas consider more influencing factors and analyze the shear contribution of each influencing factor more comprehensively. The predicted values are most consistent with the test values with the least dispersion, which can predict the shear bearing capacity of UHPC beams well.

5 | CONCLUSIONS

Shear capacity tests were conducted on eight UHPC I-shape beams to analyze the effects of reinforcement ratio, stirrup ratio and shear-to-span ratio on the shear strength and performance of the beams. Based on the test results of this study and other seven literatures, formulas from different codes and researchers were examined and the most accurate formula for calculating the shear capacity of UHPC beams was recommended. The following conclusions were drawn from the analysis of the test results:

1. The stirrup can effectively reduce the stress concentration caused by the uneven distribution of steel fibers and reduce cracks; and the GFRP bar reinforced UHPC beams can be changed from diagonal tension failure to diagonal compression failure or flexural failure.
2. Under the same load, the mid-span deflection and shear diagonal crack width of GFRP bar reinforced

UHPC beams decrease with the increase of reinforcement ratio or stirrup ratio, and the greater the shear span depth ratio, the more significant the decrease of mid-span deflection and crack width.

3. The shear capacity of GFRP bar reinforced UHPC beams increases with the increase of stirrup ratio and reinforcement ratio, but decreases with the increase of shear span depth ratio. The stirrup ratio increased from 0.0% to 0.67% and the reinforcement ratio increased from 1.4% to 2.3%, the maximum shear load capacity of the beam increased by 31.9% and 29.3% respectively. The larger the shear span depth ratio, the more significant the pinning effect of longitudinal bars on UHPC beams and the restraining effect of stirrup on UHPC and GFRP bars.
4. It is found that the calculated values of JSCE-2006 codes matches the best to the experimental values among the codes from various countries; Moreover, the calculation models proposed by Thiemicke, Kwak, and Jin are more accurate, which can well predict the shear capacity of UHPC beams.

ACKNOWLEDGMENTS

This research was financially supported by Natural Science Foundation of China (Grant No. 52022024), National Natural Science Foundation of Guangxi (Grant No. 2018GXNSFAA281188), Natural Science Foundation of China (Grant No. 51968013), Guang Xi Key Laboratory of New Energy and Building Energy Saving (Grant No. 22-J-21-14). The authors wish to acknowledge the sponsors. However, any opinions, findings, conclusions and recommendations presented in this paper are those of the authors and do not necessarily reflect the views of the sponsors.

CONFLICT OF INTEREST

The authors declare that they have no known competing financial interests or personal relationships that could have appeared to influence the work reported in this paper.

DATA AVAILABILITY STATEMENT

The data that support the findings of this study are available from the corresponding author upon reasonable request.

ORCID

Feng Fu  <https://orcid.org/0000-0002-9176-8159>

REFERENCES

1. Shin S, Seo D, Han B. Performance of concrete beams reinforced with GFRP bars. *J Asian Archit Build Eng.* 2009; 8(1):197–204.

2. Kocaoz S, Samaranyake VA, Nanni A. Tensile characterization of glass FRP bars. *Compos B Eng*. 2005;36(2):127–34.
3. Wille K, Naaman AE, Parra-Montesinos E. Ultra-high performance concrete and fiber reinforced concrete: achieving strength and ductility without heat curing. *Mater Struct*. 2012;45:309–24.
4. Wang W, Liu J, Agostini F, Davy CA, Skoczylas F, Corvez D. Durability of an ultra high performance fiber reinforced concrete (UHPFRC) under progressive aging. *Cem Concr Res*. 2014;55:1–13.
5. Yoo D-Y, Shin HO, Yang JM, Yoon YS. Material and bond properties of ultra high performance fiber reinforced concrete with micro steel fibers. *Compos B Eng*. 2014;58:122–33.
6. Cao X, Ren YC, Zhang L, Jin LZ, Qian K. Flexural behavior of ultra-high-performance concrete beams with various types of rebar. *Compos Struct*. 2022;292:115674.
7. Qian K, Geng S-Y, Liang S-L, Fu F, Yu J. Effects of loading regimes on the structural behavior of RC beam-column sub-assemblages against disproportionate collapse. *Eng Struct*. 2022;251:113470.
8. Weng Y-H, Qian K, Fu F, Fang Q. Numerical investigation on load redistribution capacity of flat slab substructures to resist progressive collapse. *J Build Eng*. 2020;29:101109.
9. Wu X, Han SM. First diagonal cracking and ultimate shear of I-shaped reinforced girders of ultra high performance fiber reinforced concrete without stirrup. *Int J Concr Struct Mater*. 2009;3(1):47–56.
10. Baby F, Marchand P, Toutlemonde F. Shear behavior of ultra-high performance fiber-reinforced concrete beams. I: Experimental investigation. *J Struct Eng*. 2015;140(5):04013111.
11. Chen B, Qianwen WU, Huang Q, et al. Experimental study on shear behavior of reinforced ultra-high performance concrete beams. *J Fuzhou Univ (Nat Sci)*. 2018;46(04):512–7.
12. Xu H, Deng Z, Chen C, et al. Experimental study on shear strength of ultra-high performance fiber reinforced concrete beams. *Chin Civil Eng J*. 2014;47(12):91–7.
13. Liang X, Wang Z, Yu J, et al. Study on shear behavior and shear bearing capacity of UHPC beams with stirrups. *Chin Civil Eng J*. 2018;51(10):56–67.
14. Qi JN, Ma ZJ, Wang J, et al. Post-cracking shear strength and deformability of HSS-UHPFRC beams. *Struct Concr*. 2016;17(6):1033–46.
15. Xia J, Mackie KR, Saleem MA, Mirmiran A. Shear failure analysis on ultra-high performance concrete beams reinforced with high strength steel. *Eng Struct*. 2011;33(12):3597–609.
16. Voo YL, Foster SJ, Gilbert RI. Shear strength of fiber reinforced reactive powder concrete prestressed girders without stirrups. *J Adv Concrete Technol*. 2006;4(1):123–32.
17. Voo YL, Poon WK, Foster SJ. Shear strength of steel fiber-reinforced ultra high-performance concrete beams without stirrups. *J Struct Eng*. 2010;136(11):1393–400.
18. Jin L-Z, Chen X, Fu F, et al. Shear strength of fiber reinforced reactive powder concrete I-shaped beam without stirrup. *Mag Concr Res*. 2019;72(21):1–39.
19. Zheng H, Fang Z, Chen B. Experimental study on shear behavior of prestressed reactive powder concrete I-girders. *Front Struct Civil Eng*. 2019;13(3):618–27.
20. Wang L, Shen N, Zhang M, Fu F, Qian K. Bond performance of steel-CFRP bar reinforced coral concrete beams. *Construct Build Mater*. 2020;245:118456.
21. Wang L, Song Z, Yi J, Li J, Fu F, Qian K. Experimental studies on bond performance of BFRP bars reinforced coral aggregate concrete, *international journal of concrete*. *Struct Mater*. 2019;13(1):52–9.
22. Chen X, Wan D, Jin L, Qian K, Fu F. Experimental studies and microstructure analysis for ultra high-performance reactive powder concrete. *Construct Build Mater*. 2019;229:116924.
23. Ultra-high Performance Fiber Reinforced Concrete [interim recommendations, revised edition]. France: AFGC Publication Press; 2013.
24. Recommendations for Design and Construction of Ultra High Strength Fiber Reinforced Concrete Structures (draft). Japan: Japan Society of Civil Engineers Press; 2006.
25. Brühwiler E. Swiss standard SIA 2052 UHPFRC: Materials, Design and Application. 4th International Symposium on Ultra-High Performance Concrete and High Performance Materials, Kassel, Germany, March 9-11. 2016. pp 1205–1209.
26. Nielsen MP. *Limit Analysis and Concrete Plasticity*. 2nd ed. Boca Raton: CRC Press; 1998.
27. Kwak Y, Eberhard M, Kim W, et al. Shear strength of steel fiber-reinforced concrete beams without stirrups. *ACI Struct J*. 2002;99(4):530–8.
28. Lim W-Y, Hong S-G. Shear strength of ultra-high performance fiber-reinforced concrete beams. 4th International Symposium on Ultra-High Performance Concrete and High Performance Construction Materials. Kassel: Kassel University Press; 2016:56–7.
29. Thiemicke J, Fehlinge E. Proposed model to predict the shear strength of UHPC-beams with combined reinforcement. 4th International Symposium on Ultra-High Performance Concrete and High Performance Construction Materials. Kassel: Kassel University Press; 2016:62–3.
30. Fu F, Parke GAR. Assessment of the progressive collapse resistance of double-layer grid space structures using implicit and explicit methods. *Int J Steel Struct*. 2018;18(3):831–42.
31. Qian K, Lan X, Li Z, Li Y, Fu F. Progressive collapse resistance of two-storey seismic configured steel sub-frames using welded connections. *J Constr Steel Res*. 2020;170:106117.
32. Gao S, Guo LH, Fu F, Zhang SM. Capacity of semi-rigid composite joints in accommodating column loss. *J Construct Steel Res*. 2017;139(12):288–301.
33. Fu F, Lam D, Ye J. Moment resistance and rotation capacity of semi-rigid composite connections with precast hollowcore slabs. *J Constr Steel Res*. 2010;66(3):452–61.
34. Yavas A, Goker CO. Impact of reinforcement ratio on shear behavior of I-shaped UHPC beams with and without fiber shear reinforcement. *Materials*. 2020;13(7):1525.
35. Yang IH, Joh C, Kim BS. Shear behaviour of ultra-high-performance fiber-reinforced concrete beams without stirrups. *Mag Concr Res*. 2012;64(11):979–93.
36. JSCE. In: Machida A, editor. Recommendation for Design and Construction of Concrete Structures using Continuous Fiber Reinforcing Materials. Tokyo: Japan Society of Civil Engineers, Concrete Engineering Series 23; 1997. p. 325.
37. Code for the Design and Construction of Building Structures with Fiber-Reinforced Polymers. Toronto: (CAN/CSA/S806-12), Canadian Standard Association; 2012. p. 198.
38. Guide for the Design and Construction of Structural Concrete Reinforced with Fiber-Reinforced Polymer (FRP) (ACI 440. 1R-15). American Concrete Institute, Farmington Hills, 2015.

39. Ashaour AS. Shear behaviour of high-strength fiber reinforced concrete beams. *ACI Struct J*. 1992;89(2):176–84.
40. ACI Committee 318 Building code requirements for structural concrete (ACI318-14) and commentary. Farmington Hills: American Concrete Institute; 2014.
41. Eurocode 2: Design of Concrete Structures—Part 1-1: General Rules and Rules for Buildings. Brussels, Belgium: European Committee for Standardization; 2004.
42. Ali HM, Alamir JSA, Hamad NT. First diagonal cracking and ultimate shear of reactive powder concrete T-beams without stirrups. *J Eng Sustain Dev*. 2014;18(5):149–64.
43. Rebeiz KS. Shear strength prediction for concrete members. *J Struct Eng*. 1999;125(3):301–8.
44. Zagon R, Matthys S, Kiss Z. Shear behaviour of SFR-UHPC I-shaped beams. *Construct Build Mater*. 2016;124:258–68.
45. Meszoely T, Randl N. Shear behavior of fiber-reinforced ultra-high performance concrete beams. *Eng Struct*. 2018;168:119–27.

AUTHOR BIOGRAPHIES



Xia Cao, College of Civil Engineering and Architecture, Guilin University of Technology, Guilin, China.
Email: 2002015@glut.edu.cn



Dabo He, College of Civil Engineering and Architecture, Guilin University of Technology, Guilin, China.
Email: 15278278996@163.com



Kai Qian, College of Civil Engineering and Architecture, Guilin University of Technology, Guilin, China.
Email: qiankai@glut.edu.cn



Feng Fu, Department of Engineering, School of Science and Technology, City, University of London, London, EC1V,0HB UK.
Email: feng.fu.1@city.ac.uk



Xiao-Fang Deng, College of Civil Engineering and Architecture, Guilin University of Technology, Guilin, China.
Email: dengxiaofang@glut.edu.cn



Lei Wang, College of Civil Engineering and Architecture, Guilin University of Technology, Guilin, China.
Email: 2006009@glut.edu.cn

How to cite this article: Cao X, He D, Qian K, Fu F, Deng X-F, Wang L. Shear behavior of glass FRP bars-reinforced ultra-high performance concrete I-shaped beams. *Structural Concrete*. 2022. <https://doi.org/10.1002/suco.202100801>